Push−Pull Bithienyl Chromophore with an Unusual Transverse Path of Conjugation

Rocío Ponce Ortiz, Reyes Malavé Osuna, Víctor Hernández, and Juan T. López Navarrete*

Department of Physical Chemistry, University of Málaga, 29071-Málaga, Spain

Barbara Vercelli and Gianni Zotti

Institute for Energetics and Interphases-IENI CNR, C.so Stati Uniti, 4-35127 Padova, Italy

Víktor V. Sumerin, Elizabeth S. Balenkova, and Valentine G. Nenajdenko*

Department of Chemistry, Moscow State University, 119899-Moscow, Russia

Received: October 9, 2006; In Final Form: November 23, 2006

The synthesis, structure, and electronic properties of a novel cross-conjugated 10*H*-bisthienodithiocin-10-dicyanoethylene are reported. The X-ray single-crystal structure of the compound reveals a nonplanar conformation. The FT-IR and FT-Raman spectra of the compound show a great resemblance, which is a spectroscopic observation common to many push−pull systems. The UV−vis spectrum in $CHCl_3$ displays a strong absorption at 370 nm accompanied by a shoulder at 430 nm so that the optical gap is 2.88 eV. On the other hand, the electrochemical gap amounts to 2.38 V. DFT and TDDFT quantum chemical calculations, at the B3LYP/6-31G** level, have been also performed to (i) determine the minimum-energy molecular structure, (ii) gain knowledge about the equilibrium atomic charges distribution, the topologies, and absolute energies of the frontier molecular orbitals around the gap and about the molecular vibrations which give rise to the most outstanding Raman bands experimentally evidenced, and (iii) to analyze the nature of the vertical one-electron excitations associated to the strongest UV−vis absorptions.

I. Introduction

The structural, electronic, and optical properties of conjugated organic molecules and their derived oligomers and polymers have attracted widespread attention in materials science in recent years.[1] Linearly π-conjugated systems, of which polyacetylene,[2] poly(*p*-phenylenevinylene)s,[3] and polythiophenes[4] are well-known examples, have received by far the most attention; and the electronic and spectroscopic properties of their charged species, generated by chemical or electrochemical doping, have been the subject of extensive investigations. The importance of studying the structure/property relationships on well-defined oligomeric models of these linearly conjugated polymers has been emphasized by several authors;[5] the benefits include precisely defined molecular structures free of any kind of defect, ease of purification, solubility, and tractability. However, alternative ways of conjugation,[6,7] such as σ-conjugation found in polysilanes,[8] $\sigma-\pi$-conjugation in oligo(cyclohexylidene)s[9,10] and silylene−arylene polymers,[11,12] and homoconjugation in diphenylpropanes, diphenylsilanes,[13,14] and 7,7-diarylnorbornanes[15] can also constitute the basis of interesting electronic features.

Cross-conjugation is a type of conjugation which has deserved only a little attention in materials research; it can be generally defined as the situation in which two unsaturated fragments are not directly linked to each other but through a third unsaturated moiety.[16] 3-Methylene-1,4-pentadiene, benzophenone, and 1,1-diphenylethene are simple examples of cross-conjugated molecules. This type of conjugation is at present receiving increasing interest as illustrated by the design of dendralene-based[17,18] and enediyne-based[19−21] systems. In the few cases in which a homologous set of oligomers was available, the main conclusion was that cross-conjugation does not result in a fairly large π-electron delocalization but the electronic properties are essentially determined by the longest linear π-conjugated fragment.[18,22]

After a recent report by some of us regarding the synthesis of a series of annulated oligothiophenes,[23] we decided to react the compound labeled as **4** with malononitrile. The resulting product was a novel "bithiophene" material with its two innermost α,α'-positions bridged by a dicyanoethylene group, whereas the innermost β,β'-positions were connected through a $-S-CH_2-S-$ bridge (see Scheme 1). This novel "bithiophene" displays a nice orange color seemingly due to the intramolecular charge transfer from the electron-rich $-S-CH_2-S-$ side chain toward the electron-deficient $=C(CN)_2$ moiety as well as the cross-conjugation between both thienyl rings and the $=C(CN)_2$ group (just like in benzophenone). In this contribution we report on the synthesis and spectroscopic characterization of this new compound (hereafter referred to as **1b**) in comparison with an isomer (**1a** in Scheme 1) in which the $-S-CH_2-S-$ and $=C(CN)_2$ electroactive groups are connected to the thienyl units in the opposite fashion, thus leading to a second bithienyl chromophore which still displays a push−pull character, but it is not longer cross-conjugated. The electrochemical behavior of these two compounds is also monitored by cyclic voltammetry. The experimental results are correlated with DFT and TDDFT quantum chemical calculations (at the B3LYP/6-31G** level of theory) about the minimum-energy molecular structure, the equilibrium atomic charges distribution, topologies, and

* Corresponding authors: E-mail: teodomiro@uma.es. (J.T.L.N.); nen@acylium.chem.msu.ru (V.G.N.).

10.1021/jp0666176 CCC: $37.00
Published on Web 01/18/2007

SCHEME 1

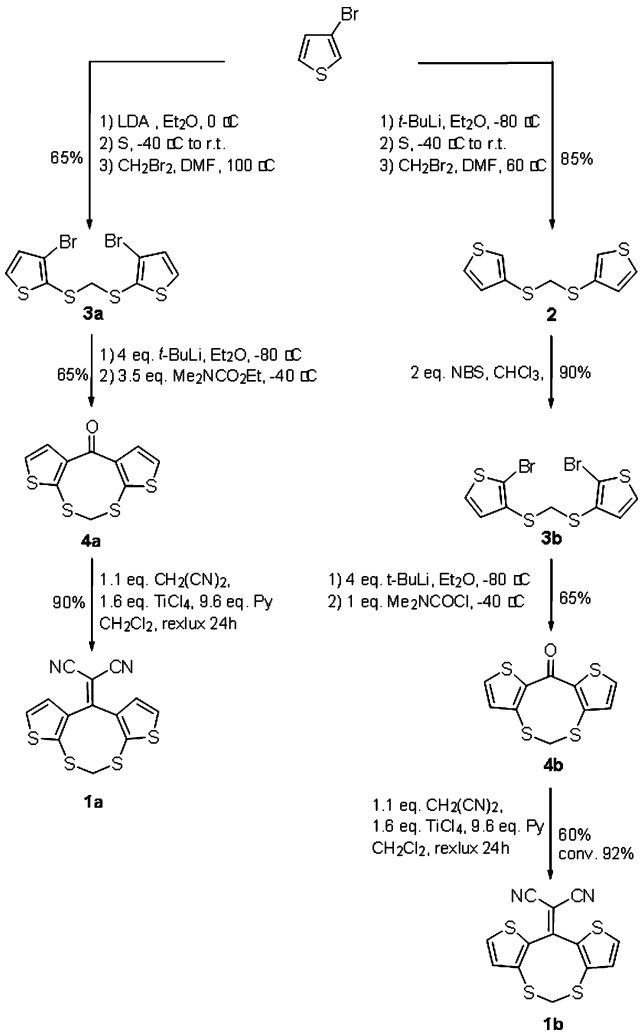

absolute energies of the frontier orbitals around the gap, IR- and Raman-active vibrations, and vertical one-electron excitations involved in the optical absorptions recorded in the visible spectral region.

II. Experimental and Computational Details

UV−vis−NIR absorption spectra in different solvents were recorded at room temperature with a Lambda 19 Perkin-Elmer dispersive spectrophotometer or by means of an Agilent 8453 instrument equipped with a diode array for fast recording of all electromagnetic absorptions in the 190−1100 nm spectral region. FT-IR spectra were recorded on a Bruker Equinox 55 spectrometer. The compound was ground to a powder and pressed in a KBr pellet. FT-IR spectra, with a spectral resolution of 2 cm^{-1}, were collected over an average of 50 scans. Interference from atmospheric water vapor was minimized by purging the instrument with dry argon before starting the data collection. FT-Raman scattering spectra were collected on a Bruker FRA 106/S apparatus with a Nd:YAG laser source (λ_{exc} = 1064 nm) in a backscattering configuration. The operating power for the exciting laser radiation was kept to 100 mW in all the experiments. Samples were analyzed as pure solids in sealed capillaries and dilute CH_2Cl_2 solutions (supplied by Aldrich with analytical grade). Typically, 1000 scans with 2 cm^{-1} spectral resolution were averaged to optimize the signal-to-noise ratio.

Variable temperature experiments were carried out using a Specac P/N 21525 cell provided with interchangeable pairs of NaCl or quartz windows for transmission studies. The variable temperature cell consists of a surrounding vacuum jacket (0.5 torr), which contains a combination of a refrigerant dewar and a heating block as the sample holder. The cell was equipped with a copper−constanton thermocouple (for temperature monitoring purposes) that allows any temperature from −150 to +210 °C (123−483 K) to be achieved. The sample was inserted into the heating block part of the dewar/cell holder assembly in the form of a KBr pellet. Spectra were recorded after waiting for thermal equilibrium at the sample, which typically required 20 min for every increment of 10 °C.

Crystals were grown by slow evaporation of solvent at room temperature. The solvents used in each case were C_2H_5OH for **1a** and CH_2Br_2 for **1b**. All X-ray diffraction patterns were collected at 293 K on an Enraf Nonius CAD4 diffractometer (Mo Kα, 0.71073 Å). The structures were previously solved with direct methods and further refined with a full-matrix least-squares technique by using the SHELXL-97 program package.[24] All non-hydrogen positions were refined anisotropically, whereas those of the hydrogen atoms were found in the difference map.

All electrochemical measurements were performed in acetonitrile of reagent grade (Uvasol, Merck) with a water content <0.01%. Tetrabutylammonium perchlorate of reagent grade was purchased from Fluka and used as the supporting electrolyte (0.1 M) as received, without further purification. Cyclic voltammetry analysis was run in three-electrode cells at 25 °C on solutions previously deaerated by N_2 bubbling, keeping a continuous nitrogen gas flow during all the experiment. The counter electrode was platinum; the reference electrode was silver/0.1 M silver perchlorate in acetonitrile (0.34 V vs SCE). The voltammetric apparatus (AMEL, Italy) included a 551 potentiostat modulated by a 568 programmable function generator, coupled to a 731 digital integrator. The working electrode for cyclic voltammetry was a platinum (0.003 cm^2) minidisk electrode. To record the UV−vis−NIR absorption spectra of solution-cast solid films, 0.8 cm × 2.5 cm ITO sheets (≈80% transmittance, ≈20 ohms/sq standard square resistance, from Balzers, Liechtenstein) were used. FT-IR spectra of polymer films were recorded in a reflection−absorption configuration on the working electrode (a platinum sheet electrode) by means of a Perkin-Elmer 2000 FT-IR spectrometer.

DFT calculations were carried out using revision A.7 of the GAUSSIAN 03 program package[25] running on an SGI Origin 2000 computer. Calculations of the optimized geometry, electronic excitation energies, and vibrational spectra were performed on a single molecule in the vacuum using the Becke's three-parameter B3LYP exchange-correlation functional.[26] The 6-31G** basis set[27] was chosen as a compromise between accuracy and applicability to large molecules. Geometries were optimized with the eigenvector-following routine. In order to keep the molecular symmetry, appropriate geometry constraints were imposed on the bond lengths, bond angles, and dihedral angles. Force calculations were run to ensure that the resulting geometries were minima on the potential energy surface and to calculate vibrational spectra. Nonetheless, the geometry optimization without symmetry constraints could perhaps render a slightly more stable twisted conformer.

Vertical excitation energies were computed for the 15 lowest-energy electronic excited states by using the time-dependent DFT (TDDFT) approach.[28−30] This approach has been widely used to study the electronic spectra of large π-conjugated systems such as polyenes,[31] polycyclic aromatic hydrocarbons,[32,33] fullerenes,[34] α-oligomers of thiophene, *p*-phenylene, *p*-phenylenevinylene,[35] porphyrin-type macrocycles, oligo-

mers,[36,37] and so on. Standard hybrid functionals such as BLYP and B3LYP provide excitation energies that are roughly within 0.3 eV to the experimental data. Despite these encouraging results, the TDDFT approach should be used with caution, since predicted excitation energies can be affected by quite different errors. Overestimations/underestimations by 0.4−0.7 eV are not unusual,[31,32e,f] which can lead to misassignments when trying to provide a full interpretation of the whole electronic spectrum.[38] Molecular orbital contours were plotted using Molekel 4.3.[39]

The calculated harmonic vibrational frequencies were scaled down uniformly by a factor of 0.96 as recommended by Scott and Radom.[40] All the theoretical vibrational data quoted along the manuscript thus correspond to scaled values. The theoretical infrared and Raman spectra were obtained by convoluting the scaled frequencies with Gaussian functions (10 cm^{-1} width at the half-height). The height of the Gaussians was determined from the IR intensities and Raman scattering activities calculated for the corresponding IR- and Raman-active normal modes. The IR intensities were evaluated from the dipole moment derivatives with respect to the normal coordinates, while molecular polarizability derivatives for Raman activities were deduced from the numerical differentiation of the analytical dipole moment derivatives with respect to the applied electric field.

III. Results and Discussion

III.a. Synthesis and Purification. Herein we describe a short synthesis of two yet unknown isomeric 10*H*-bisthienodithiocin-10-ylidenemalononitriles. The synthesis of **1a**, **1b** was carried out according to Scheme 1 starting from cheap commercially available 3-bromothiophene. Earlier, we have elaborated an effective procedure for preparation of two isomeric 10*H*-bisthienodithiocin-10-ones (**4a**, **4b**).[23] The key step of the method involves cyclization of methylene-bis(thio)-bisbromothiophenes (**3a**, **3b**).

The intermediates for the synthesis of **4a** and **4b** are isomeric bisdibromothienylsulfanyl-methanes (**3a**, **3b**). We elaborated a one-pot procedure for the preparation of **3a** from 3-bromothiophene.[41] The treatment of 3-bromothienyl-2-lithium with sulfur followed by the addition of 1 equiv of dibromomethane gave target **3a** in 65% yield. While using the calculated 0.5 equiv of dibromomethane the yield of **3a** was less than 35%. Isomeric **3b** was prepared in two steps from 3-bromothiophene via **2**. 3-Thienyllithium was treated with 1 equiv of sulfur, and the resulting lithium thiolate was alkylated with 0.5 equiv of dibromomethane to give after distillation in portions (no more than 0.05 mol) **2** in 85% yield. On the second stage consequent treatment of **2** with 2 equiv of NBS gives **3b** in 90% yield. Ketones **4a** and **4b** have been prepared from the lithium derivatives and *N*,*N*′-dimethylethylcarbamate and *N*,*N*′-dimethylcarbamyl chloride accordingly, which are known as one of the best and very convenient reagents for the synthesis of symmetric aryl ketones.[42,43] Lithiation of **3a** and **4b** using 4 equiv of *t*-BuLi followed by addition of 3.5 equiv of *N*,*N*′-dimethylethylcarbamate and 0.5 equiv of *N*,*N*′-dimethylcarbamyl chloride gave **4a** and **4b** correspondingly in 65% yield (optimization of the reaction conditions to afford the synthesis of **4a** is outlined in Figure S1 in the Supporting Information). Finally, target compounds **1a** and **1b** were obtained by the condensation of 10*H*-bisthienodithiocin-10-one (**4a**, **4b**) with malononitrile in the presence of $TiCl_4$.[44]

III.b. Crystal Structures. The structures of **1a** and **1b** were determined by single-crystal X-ray analysis. The two compounds display a twisted molecular conformation in the solid state, and for some molecules of **1a** atom C5A2 was found to be statistically disordered over two different spatial orientations, denoted as C5A2(1) and C5A2(2) in Figure 1.

*III.b.1. Compound **1a*:** yellow prism, monoclinic, 0.32 × 0.13 × 0.11 mm^3, *C*2/*c*, $Z = 12$. Cell dimensions: $a = 17.264(3)$, $b = 9.878(2)$, $c = 24.127(5)$ Å; $\alpha = 90.00°$, $\beta = 91.45(3)°$, $\gamma = 90.00°$, $V = 4113.2(14)$ $Å^3$, $2\theta_{max} = 48.98$, $d_{calcd} = 1.543$ $g\cdot cm^{-3}$. Of 3539 reflections, 3417 were independent ($R_{int} = 0.0154$), 262 parameters, R1 = 0.0390 (for reflection with $I > 2\theta(I)$), wR2 = 0.0993 (for all reflections).

*III.b.2. Compound **1b*:** yellow prism, monoclinic, 0.31 × 0.22 × 0.12 mm^3, *C*2/*c*, $Z = 4$. Cell dimensions: $a = 16.357(3)$, $b = 9.943(2)$, $c = 10.168(2)$ Å; $\alpha = 90.00°$, $\beta = 123.73(3)°$, $\gamma = 90.00°$, $V = 1375.3(5)$ $Å^3$, $2\theta_{max} = 55.94$, $d_{calcd} = 1.538$ $g\cdot cm^{-3}$. Of 1712 reflections, 1658 were independent ($R_{int} = 0.0364$), 101 parameters, R1 = 0.0308 (for reflection with $I > 2\theta(I)$), wR2 = 0.0963 (for all reflections).

III.c. Structure Calculations. DFT//B3LYP/6-31G** model chemistry predicts a twisted minimum-energy structure, for both **1a** and **1b**, as the highly prevailing geometry for the isolated entity in the vacuum (see Figure 2), with the two sulfur atoms of the electron-rich −S−CH_2−S− bridge pointing out at either side of the bithienyl core. These two gas-phase theoretical structures are in good agreement with those derived from the experimental single-crystal X-ray diffraction data, although the optimized B3LYP/6-31G** bond lengths are in general longer than the experimental quantities (see Tables S3 and S8 in the Supporting Information). Among the factors that primarily determine the relative stability of the conformers of these two isomeric eight-membered bisthienodithiocin unsaturated heterocycles are angle strain, lone pair−lone pair repulsion, π-electron−lone pair repulsion, and conjugative interactions between the −S−CH_2−S− and C═C$(CN)_2$ side groups and the thienyl rings.

Although the two formally C−C single bonds connecting the C═C$(CN)_2$ acceptor group to the inner α-positions of the thienyl rings of **1b**, with optimized B3LYP/6-31G** bond lengths of 1.467 Å, belong to the long fraction of C(sp^2)−C(aryl) bonds, for which the average is 1.470 Å,[45] the olefinic C═C bond length of 1.394 Å is however rather long as compared with the C═C bond length of 1.339 Å in conjugated aryl-substituted alkenes.[45] Judging merely from the optimized bond lengths, the C═C$(CN)_2$ group seems to be somewhat more conjugated in **1b** than in **1a**, although the degree of conjugation is less pronounced than in α-linked thiophene-based π-conjugated heteroquinoid analogues of TCNQ.[46] We also see that, although the CC bonds of the thienyl rings have normal B3LYP/6-31G** lengths, the inner C_α═C_β distance of both isomers is significantly larger than the outer one by nearly 0.03 Å. The mean single−double CC bond length alternation pattern (BLA) parameter for each thienyl ring, computed at the B3LYP/6-31G** level of theory as $r(C_3-C_4) - 0.5r(C_2{=}C_3) - 0.5r(C_1{=}C_4)$, amounts to +0.062 Å for **1a** and +0.040 Å for **1b**, in agreement with an increasing degree of quinoidization from the former to the latter bisthienodithiocin.

As for the electrostatic picture of **1b**, the B3LYP/6-31G** net atomic charge over the −S−CH_2−S− bridge, calculated using natural population analysis (NPA), amounts to +0.351 *e* (see Figure 3), which is balanced by negative charges over each thienyl ring (−0.051 *e*) and the dicyanoethylene acceptor group (−0.247 *e*). DFT calculations thus predict a partial degree of intramolecular charge transfer for **1b** from the electron-rich −S−CH_2−S− bridge toward both the thienyl rings and the C═C$(CN)_2$ acceptor moiety. As a result of the ground-state

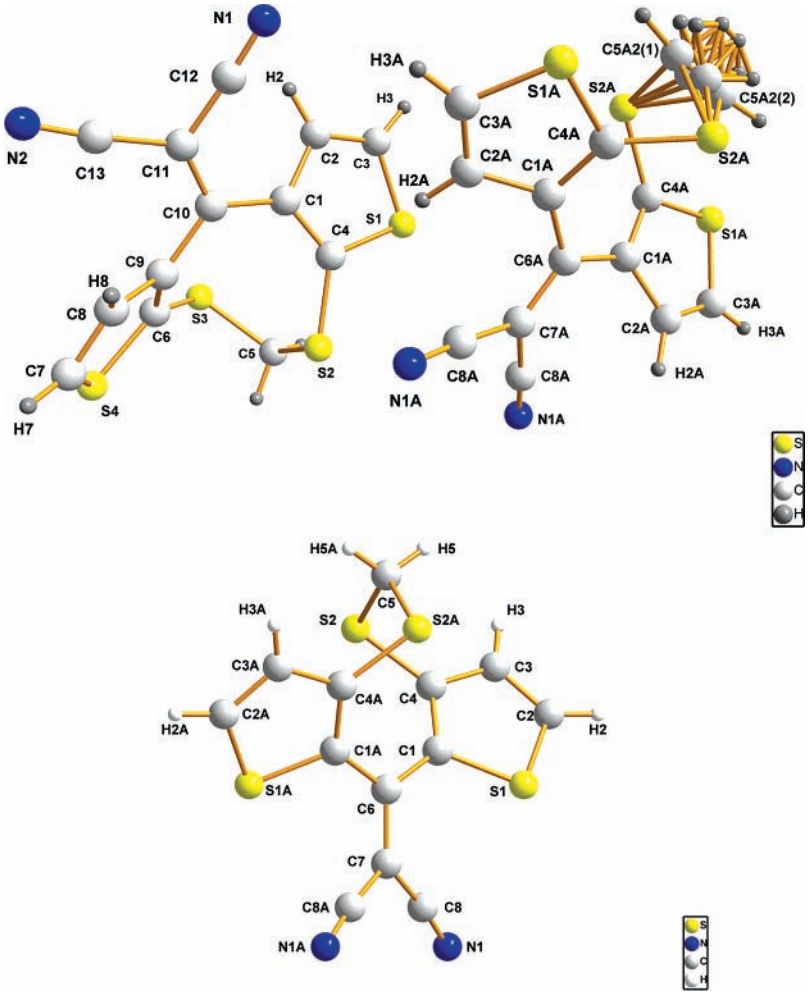

Figure 1. X-ray structures of **1a** and **1b**.

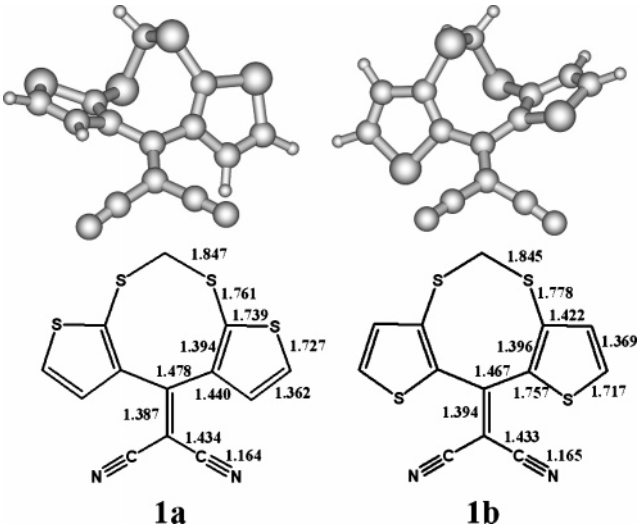

Figure 2. Lateral views of the optimized molecular structures of **1a** and **1b** and B3LYP/6-31G** values for selected skeletal bond lengths.

polarization, the molecular dipolar moment calculated for this compound amounts to 7.57 D. Regarding the second isomer, **1a**, the B3LYP/6-31G** NPA charges over the $-S-CH_2-S-$ bridge and the thienyl units now increase to +0.408 and −0.119 *e*, respectively, whereas that over the $C{=}C(CN)_2$ acceptor side group decreases to −0.171 *e* (in agreement with a lesser ICT or push−pull character).

III.d. Electronic Absorption Spectra. Figure 4 shows the UV−vis−NIR spectra recorded for **1a** and **1b** in CH_2Cl_2 solution. The spectrum of **1b** displays a broad feature extending from near 300 to 470 nm, with a maximum at 370 nm (3.35 eV, $\epsilon = 13\,386\ M^{-1}\ cm^{-1}$) and a distinct shoulder near 430 nm ($\epsilon = 6518\ M^{-1}\ cm^{-1}$). The corresponding spectra in CH_3CN and DMSO solutions show a quite similar profile to that in CH_2Cl_2 and only a moderate shift of the main absorption band (364 nm in CH_3CN and 375 nm in DMSO). At first sight, the electronic absorption of **1b** is close to the $\pi-\pi^*$ transition common α-linked aromatic oligothiophenes display in the visible spectral region at ≈350−450 nm. In this regard, the $\pi-\pi^*$ absorption of α-terthiophene occurs at 355 nm (3.49 eV), whereas it red-shifts to 390 and 432 nm (3.18 and 2.87 eV) for quaterthiophene and sexithiophene, respectively.[46] On the other hand, the main visible absorption band of **1a** is upshifted, by ≈60 nm, up to 329 nm (3.77 eV, $\epsilon = 24\,536\ M^{-1}\ cm^{-1}$) and the distinct shoulder to 390 nm (3.18 eV, $\epsilon = 13\,163\ M^{-1}\ cm^{-1}$). This experimental finding is again in full agreement with a lesser degree of conjugation in **1a**.

To gain a deeper insight into the optical properties of **1b** we decided to perform calculations of vertical one-electron excitation energies (i.e., by considering at least the 15 lowest-energy electronic excited states) by means of the time-dependent DFT formalism on the previously optimized ground-state DFT// B3LYP/6-31G** structure. Calculations predict the appearance of two visible bands at 2.73 eV (454 nm) and 3.04 eV (408 nm) due to the HOMO → LUMO and HOMO-2 → LUMO

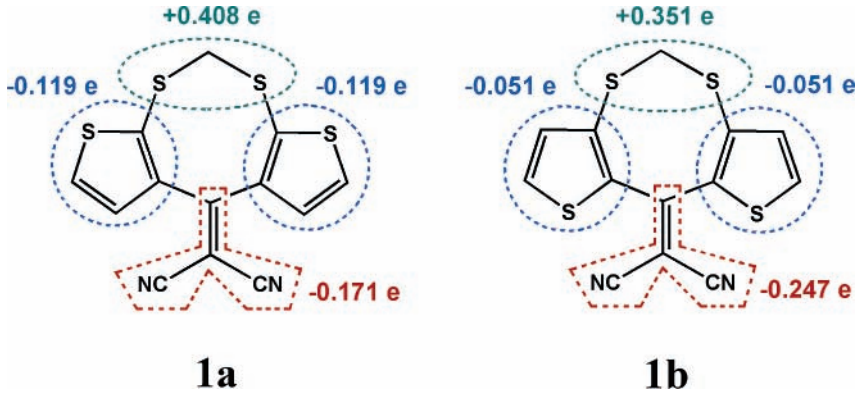

Figure 3. B3LYP/6-31G** net NPA charges on various molecular domains of **1a** and **1b**.

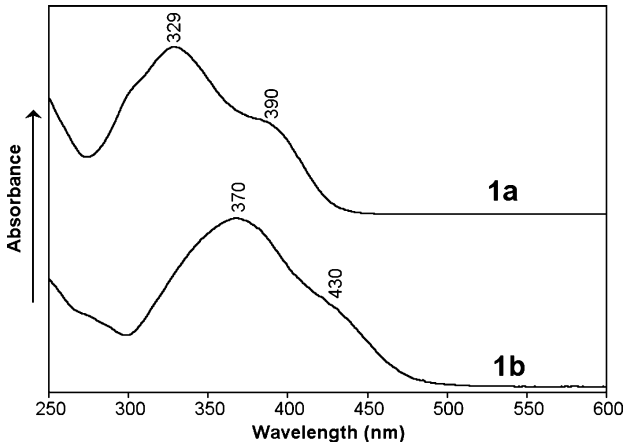

Figure 4. UV−vis absorption spectrum of **1a** and **1b** in CH_2Cl_2 solution.

transitions, with oscillator strengths of $f = 0.028$ and 0.038, respectively, together with other two stronger electromagnetic absorptions at 3.27 eV (379 nm, $f = 0.193$) and 3.56 eV (348 nm, $f = 0.103$) arising from the HOMO-1 → LUMO and the HOMO-4 → LUMO excitations, respectively.

The experimental oscillator strength, f_{expt}, for the optical absorption of **1b** at 370 nm was estimated from the conversion between the extinction coefficient and oscillator strength, $f = 4.319\ 10^{-9}$ (M cm^2)A, where A is the integrated absorption coefficient. The value of A is found by determining the area under an absorption band that is displayed as x-axis = wavenumber (cm^{-1}) against y-axis = molar absorption coefficient (M^{-1} cm^{-1}). The units of A (M^{-1} cm^{-2}) and the value of $4.319\ 10^{-9}$ M cm^2 cancel to give the dimensionless value of f_{expt}. The accurate estimate of the integrated absorption coefficient for **1b** from Figure 4 led to $f_{expt} \approx 0.471$, which is in reasonable agreement with the sum of the oscillator strengths for the four lowest-lying calculated transitions as quoted in the paragraph above, $f_{calc} = 0.362$; and this provides another piece of evidence for the quality of the TDDFT calculations.

Figure 5 displays the atomic orbital compositions and energies of the HOMO-4, HOMO-2, HOMO-1, HOMO, LUMO, and LUMO+1 levels of **1b** around the band gap region. From the TDDFT and DFT calculations we learn that the three optical absorptions at 3.04 eV (HOMO-2 → LUMO), 3.27 eV (HOMO-1 → LUMO), and 3.56 eV (HOMO-4 → LUMO) imply a partial transfer of electron density from the electron-rich aliphatic S atoms toward the electron-deficient C═C(CN)$_2$ group, through the innermost C_α═C_β bonds of the thienyl rings. These B3LYP/6-31G** calculations also evidence that the HOMO spreads over the entire chromophore, an observation

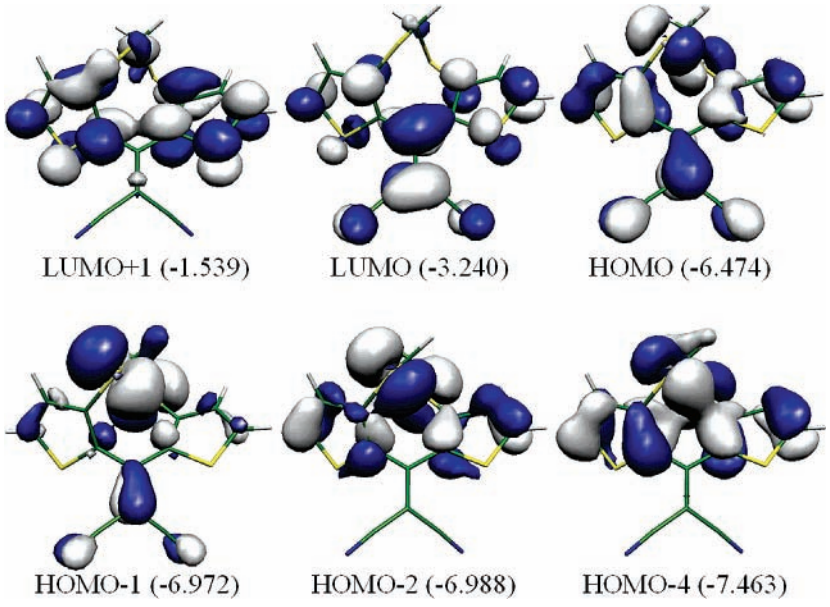

Figure 5. B3LYP/6-31G** electronic density contours (0.03 e/b^3) and absolute energies (in eV) for selected molecular orbitals of **1b** around the band gap.

which is in agreement with a quite effective conjugative interaction between the various constituting building blocks.

It usually happens that the computed TDDFT energies for vertical one-electronic transitions from doubly occupied MOs to empty MOs are predicted to be somewhat smaller than the corresponding difference between the absolute energies of both orbitals, as a consequence of the mitigated interelectronic interaction upon the single electronic excitation. This seems also be the case for the HOMO-1 → LUMO transition of **1b**: the TDDFT approach predicts a 3.27 eV electromagnetic absorption for this one-electron excitation to occur, while the B3LYP/6-31G** HOMO−LUMO gap amounts to a higher value of 3.73 eV; the 0.46 eV difference should likely be ascribed to a sizable reduction of the Coulomb interelectronic repulsion provided that the LUMO spreads over a larger molecular domain than the HOMO (see Figure 5).

The TDDFT predicted energies for the HOMO-2 → LUMO and HOMO-4 → LUMO transitions (i.e., 3.04 and 3.56 eV) are also found to be substantially lower by 0.71 and 0.66 eV, respectively, than the corresponding DFT//B3LYP/6-31G** gap; although here the origin of such stabilizations upon the corresponding single electronic excitation seems to be the result of the interplay between both Coulomb and exchange interactions since the MOs involved in each electronic transition now spread over two more closer molecular domains of the chromophore, thus giving rise to a larger overlap between them.

Some considerations of general validity can be drawn from the detailed analysis of the optical properties of **1b** provided by these TDDFT//B3LYP/6-31G** calculations. First, in spite of being very often assumed as a direct measure of the effectiveness of the π-conjugation in a system, UV−vis−NIR absorption data are not unambiguous for this purpose. For instance, when analyzing a homologous set of linear π-conjugated oligomers, it is not unusual that the optical properties reach saturation for rather short chain lengths, whereas the energy levels around the band gap region are still predicted to vary for even quite longer oligomers. For these one-dimensional α-linked chains, the Coulomb and exchange terms, which conceptually describe in an easy way the interelectronic interactions, should decrease as the number of repeating units in the chain increases (namely, this hypothetic trend of variation is related to the thought that as the oligomer grows longer the interelectronic repulsion for a given doubly occupied MO should progressively mitigate, particularly if such MO spreads over the whole π-conjugated path). Nonetheless, it is commonly found that along a given homologous series of oligomers, the narrowing of the HOMO−LUMO energy gap with increasing number of units in the π-conjugated chain is however more pronounced so that the interplay between the Coulomb and exchange integrals is less relevant in determining the energy of the singlet excited state involved in the HOMO → LUMO excitation.[47] The situation outlined here could be more troublesome when trying to derive meaningful structure/property relationships from the optical spectroscopic data of a series of alternating donor−acceptor π-conjugated cooligomers.[48] Thus, it is preferable that the analysis of the experimental UV−vis−NIR data is not merely based on the *chemical intuition*, but performed upon the light of some sort of accurate quantum chemical calculation about topologies and energies of the MOs and of the multiconfigurational character of the different UV−vis−NIR absorptions.

III.e. Electrochemical Properties. As shown in Figure 6, **1b** is reversibly reduced at $E^0_{red} = -1.05$ V in CH_3CN/0.1 M Bu_4NClO_4 solution and irreversibly oxidized at $E_p^{ox} = 1.33$ V. The electrochemical gap of **1b**, $\Delta E = 2.38$ V, is thus found to be smaller, for instance, than that reported for a perfluorinated α-sexithiophene, **PF-6T**, which also shows an amphoteric redox behavior ($\Delta E^0 = 2.81$ V).[49] However, as aforementioned, **1b** absorbs at 370 nm, whereas **PF-6T** does at 421 nm. It has been claimed in the literature that the transition energies measured from the optical spectra can provide a different conjugation picture to that suggested by the energies of the individual MOs disclosed by either cyclic voltammetry or quantum chemical calculations. This is particularly evident when studying a homologous set of cross-conjugated oligomers: the increase in the number of units might be not accompanied by a noticeable bathochromic shift of the UV−vis absorptions (i.e., the optical properties reach saturation again very quickly with chain length), whereas the redox potentials continue to vary for longer systems.[18,22,50] On the other hand, it is well-known that solvation energies change the electrochemical gap compared with the optical gap,[51] so this effect could be also attributed to this fact.

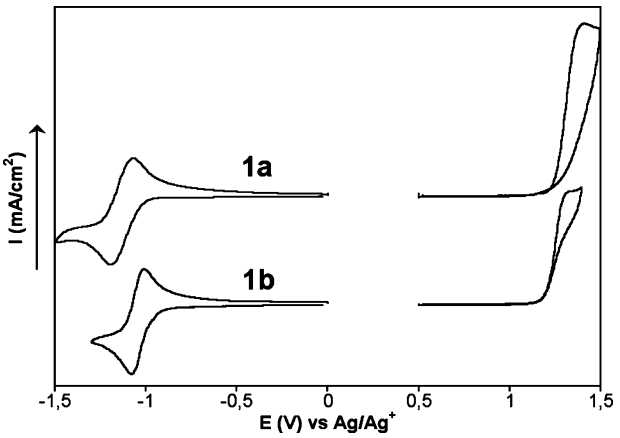

Figure 6. Cyclic voltammogram of **1a** and **1b** in 0.1 M Bu_4NClO_4/CH_3CN solution. The scan rate was 100 mV s^{-1}, and the reference electrode was Ag/0.1 M $AgClO_4$ in CH_3CN (0.34 V vs SCE).

For **1a**, the values are $E^0_{red} = -1.15$ V and $E_p^{ox} = 1.40$ V, namely, the electrochemical gap is somewhat larger than for **1b** (in agreement with the optical data). Thus, the electrochemical analysis of the two isomeric bisthienodithiocins also indicates that **1a** is less conjugated than **1b**.

No film formation was observed during the potentiostatic oxidation of **1b** but only soluble products. Bulk oxidized monomer was obtained by oxidation at 1.3 V of 32 mg in 25 mL of CH_3CN/0.1 M Bu_4NClO_4. After the passage of ca. 2.2 F mol^{-1} the orange-brown solution was evaporated, and the resulting product was separated by extraction with CH_2Cl_2/H_2O. The FT-IR spectrum of the pure **1b** monomer recorded in the form of a KBr pellet is plotted in Figure 8, whereas that collected for its oxidation product in a reflection−absorption configuration on the working electrode (see Figure 7) shows the appearance of an additional strong absorption near 1700 cm^{-1}, indicative of overoxidation. This result could be anticipated in view of the chemical structure of this cross-conjugated system: the first oxidation potential of **1b** is so high that its radical cation is prone to fast deprotonation and further oxidation.

III.f. Infrared and Raman Spectroscopic Results. The structural and conjugative properties of **1b** were further investigated with infrared and Raman spectroscopies. Figures 8 and 9 depict the solid-state FT-IR and FT-Raman spectra of **1b**, respectively. At first sight, its IR and Raman spectral profiles display an extraordinary resemblance, regarding both the positions and relative intensities of the main vibrational features. This spectroscopic behavior is common to many families of push−pull π-conjugated oligomers,[52] and it has been accounted

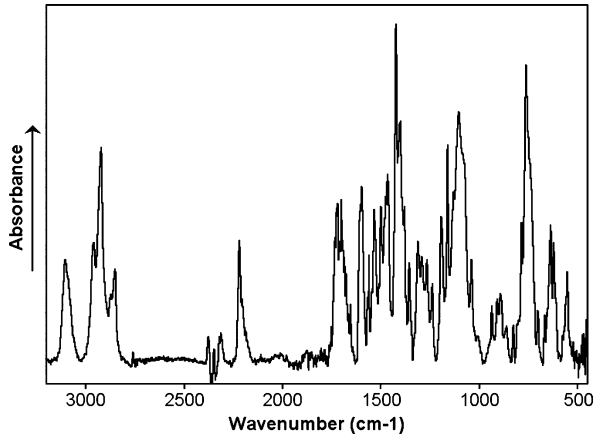

Figure 7. FT-IR spectrum collected for the oxidation product of **1b** as a film on the platinum working electrode by using a reflection−absorption configuration.

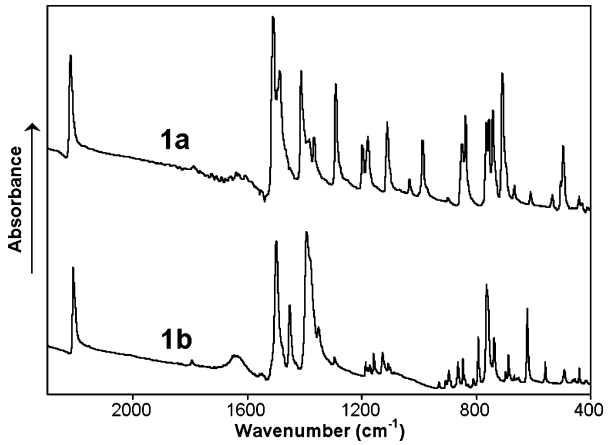

Figure 8. FT-IR spectrum of **1a** and **1b** recorded in the form of a pressed KBr pellet over probe energies of 2300−400 cm^{-1}.

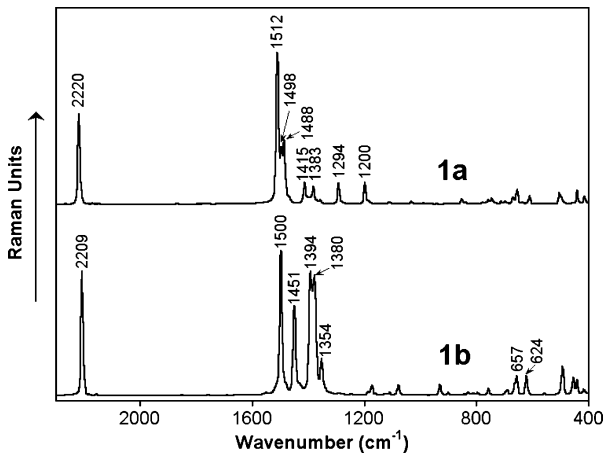

Figure 9. Solid-state FT-Raman spectrum of **1a** and **1b** over probe energies of 2300−400 cm^{-1}.

for by the fact that the large molecular dipole moment directed from the acceptor to the donor groups makes the same vibrational normal modes of the π-conjugated backbone, which give rise to the main Raman scatterings experimentally recorded to further gain an extralarge IR activity. This is due to the sizable fluxes of charge induced along the highly polarized alternating sequence of conjugated C═C/C−C bonds. Contrarily, for nonpolar centrosymmetric oligothiophenes, the mutual exclusion principle holds due to the existence of an inversion center in the middle of the system so that the Raman-active vibrations

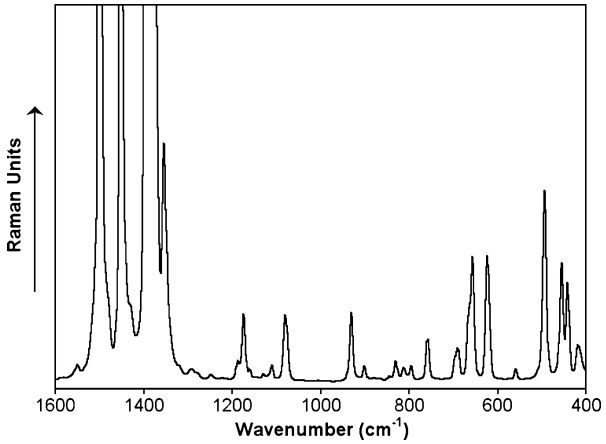

Figure 10. Enlarged profile of the FT-Raman spectrum of **1b** showing the selective enhancement of a few skeletal ν(CC) stretching vibrations between 1500 and 1300 cm^{-1} with respect to the many Raman scatterings appearing below 1000 cm^{-1}.

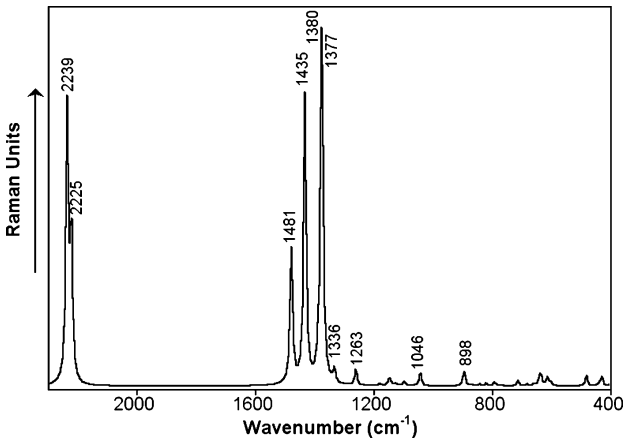

Figure 11. DFT//B3LYP/6-31G** Raman spectrum for **1b**.

become undetectable in the IR spectrum and vice versa.[47,53] Furthermore, for common aromatic oligothiophenes, the out-of-plane γ(C−H) bending modes, appearing around 800 cm^{-1}, give rise to by far the strongest IR absorptions, while for push−pull oligothiophenes, the main IR features are usually found above 1300 cm^{-1} and are associated to skeletal ν(C═C) stretching vibrations. Thus, a great resemblance between the IR and Raman spectra can be taken as a proof of effective ICT, and this should also be true for the cross-conjugated bithiophene studied here.

Let us now pay particular attention to the Raman spectral profile: as one can see, it is mainly built up of a strong scattering at 2209 cm^{-1} together with other few sharp lines between 1550 and 1350 cm^{-1}, while the remaining Raman features appearing below 1300 cm^{-1} display a significantly lower intensity. The enlarged Raman spectral profile shown in Figure 10aserves to illustrate in a more precise way this finding, which nowadays constitutes a well-documented spectroscopic characteristic to any sort of π-conjugated system (i.e., both oligomers and polymers).[54−56]

The B3LYP/6-31G** Raman spectrum of **1b** (see Figure 11) nicely accounts for the overall appearance of the experimental one, regarding the number of selectively enhanced Raman scatterings and their approximate peak positions and relative intensities. We however observe that the theoretical IR/Raman frequency values are in general lower than the experimental ones, which can be attributed to the well-known tendency of DFT calculations to overestimate π-conjugation. Anyway, the

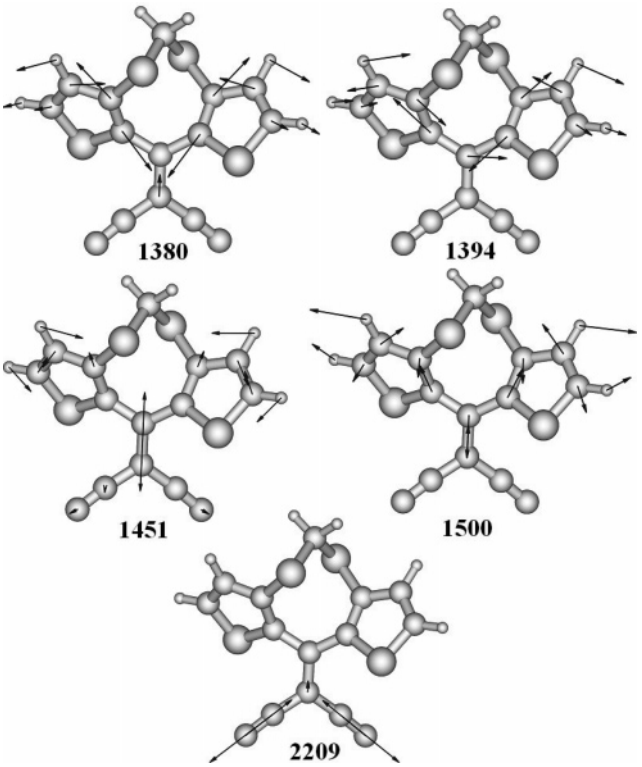

Figure 12. B3LYP/6-31G** vibrational eigenvectors associated to the main IR- and Raman-active normal modes of **1b** (experimental wavenumbers are given in cm^{-1}).

theoretical support to our experimental work allows us to propose a tentative full vibrational assignment for the main IR/Raman bands.

The in-phase C≡N stretching vibration is measured as a sharp peak at 2209 cm^{-1} in both the IR and Raman spectra. The shift toward lower frequencies of this vibration on complexation of TCNQ with electron donors has been related in the past to the degree of charge transfer in organic conducting salts, since its peak position is highly sensitive to the electron density borne by the electron-deficient C≡N groups.[57] The IR absorption due to the ν(CN) mode also largely shifts for a few novel amphoteric heteroquinoid TCNQ analogues upon oxidation/reduction of the neutral compound to their various redox forms.[58] For instance, the ν(CN) mode is measured at 2225 cm^{-1} for neutral TCNQ, at 2197 cm^{-1} for TCNQ radical anion, and at 2164 cm^{-1} for TCNQ dianion.[59,60] Under the assumption of the applicability of the data summarized in Figure 1 of ref 57a to the compounds subject of study, the electron density transferred from the thienyl−S−CH_2−S−thienyl core to the electron-withdrawing =$C(CN)_2$ moiety is estimated to be ≈0.40 *e* (namely, nearly 35% larger than the computed B3LYP/6-31G** NPA overall charge). The large involvement of the nitrile groups in the π-conjugation of **1b** can be also derived from the correlation between the rather low frequencies of their IR/Raman-active stretching modes and the corresponding values for a nonconjugated compound like commercial CH_2CN_2: 2273 cm^{-1} (IR) and 2265 cm^{-1} (Raman).

The infrared and Raman features recorded over the 1600−1300 cm^{-1} frequency range can provide useful information regarding the π-conjugational properties. As sketched in Figure 12, the strongest IR and Raman features at 1500 cm^{-1} are due to an in-phase antisymmetric ν_{asym}(C=C) stretching of the thienyl rings coupled to the stretching of the olefinic bond of the dicyanoethylene group. When **1b** becomes distorted along this molecular vibration, toward the opposite direction as shown in Figure 12, the bonding interactions in the HOMO between the three innermost C=C bonds become weaker, whereas the strong antibonding interaction in the LUMO between the carbon atoms of the olefinic double bond is largely relaxed. Therefore, the LUMO is stabilized in energy by such structural distortion at the time that the HOMO is raised up, thus leading to a narrowing of the HOMO−LUMO gap.

The three IR/Raman bands at 1451, 1394, and 1380 cm^{-1} are due to stretching vibrations of the aromatic rings: (i) that at 1451 cm^{-1} is to be assigned to the stretching of the olefinic bond of the dicyanoethylene group coupled to an in-phase antisymmetric ν_{asym}(C=C) stretching of the thienyl rings, (ii) the mode at 1394 cm^{-1} is mostly due to the out-of-phase ν_{sym}(C=C) stretching of the thenyl units, whereas (iii) the Raman scattering at 1380 cm^{-1} arises from the in-phase ν_{sym}(C=C) stretching of both aromatic rings. Finally, in this region, the IR absorption around 1354 cm^{-1}, appearing as a shoulder at the lower-energy side of the strong and sharp peak at 1394 cm^{-1}, is due to a $\delta(CH_2)$ bending of the −S−CH_2−S− bridge. From the comparison between the vibrational eigenvectors and the electronic density contours for the MOs around the band gap, we see that when **1b** is distorted along the Raman mode at 1451 cm^{-1}, toward the opposite direction as shown in Figure 12, the bonding interactions in the HOMO between the outermost C_α=C_β bonds of the thienyl rings and the olefinic double bond become weaker, whereas the strong antibonding interaction in the LUMO between the carbon atoms of the olefinic bond is relaxed. On the other hand, along the structural distortion of **1b** at 1394 cm^{-1}, the bonding interactions in the HOMO between the two C_α=C_β bonds on one thienyl ring become weaker, whereas those on the another thiophene ring become stronger. Finally, the skeletal distortion of **1b** along the Raman mode of 1380 cm^{-1} toward the same direction depicted in Figure 12 weakens the bonding interactions in the HOMO between the four C_α=C_β bonds of the electron-rich thienyl−S−CH_2−S−thienyl core, thus significantly raising up in energy this frontier orbital.

As mentioned above, the remaining Raman scatterings recorded below 1300 cm^{-1} display a comparatively much weaker intensity, since they are not involved to so large an extent into the conjugation of the systems. For instance, the Raman scatterings of **1b** at 657 and 624 cm^{-1} are due, respectively, to an in-plane δ_{ring} bending and an out-of-plane γ_{ring} folding mode of the thienyl rings. On the other hand, its two stronger IR absorptions in the low-frequency range are those recorded as a broad feature around 765 cm^{-1} and as a sharp peak at 622 cm^{-1}; the former arises from the overlap of three almost degenerate out-of-plane γ(CH) bending modes with different phases, while the latter results from the overlap of the same γ_{ring} folding vibration measured in the Raman spectrum at 624 cm^{-1} and a second IR-active γ_{ring} vibration for which the displacements of symmetry equivalent atoms from their equilibrium positions take place in opposite directions with respect to the thienyl−S−CH_2−S−thienyl backbone.

On the other hand, the lesser π-conjugation of **1a** as compared with **1b** could be anticipated in view of its quite different IR and Raman spectral profiles. Thus, the FT-IR spectrum of **1a** displays the usual appearance of any organic chemical with a covalent structure (namely, it is made up of several sharp absorptions of comparable intensities spreading over the whole spectral range), whereas only two outstanding by far Raman scatterings are measured at 2220 and 1512 cm^{-1}, accompanied by other two weaker features at 1498 and 1488 cm^{-1}. The fact that the selectively enhanced Raman-active modes appear at

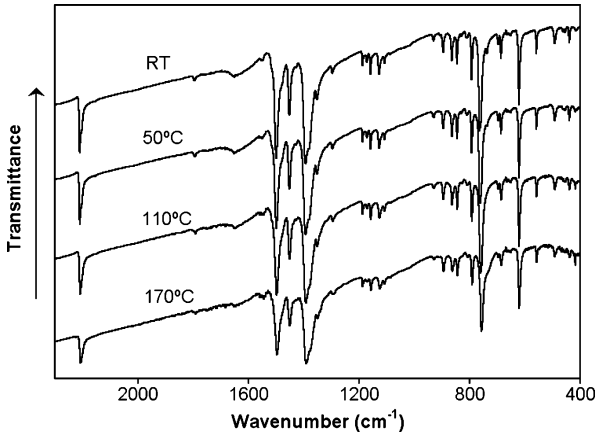

Figure 13. Thermal evolution of the FT-IR spectrum of **1b** from room temperature to 170 °C.

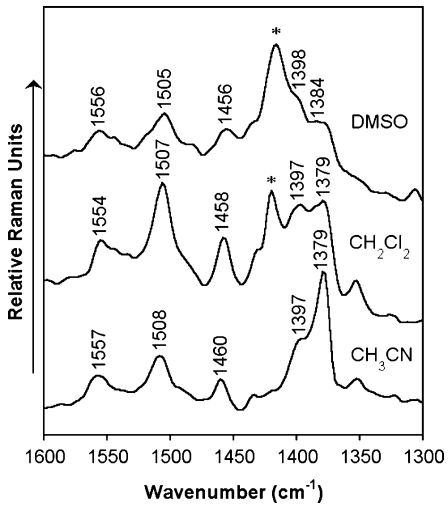

Figure 14. FT-Raman scattering profiles of **1b** as a dilute solute in CH_2Cl_2, CH_3CN, and DMSO solutions, in the 1600−1300 cm^{-1} Raman shifts spectral ranges (asterisks denote residual solvent scatterings).

significantly higher frequencies than their counterparts in **1b** is once again in agreement with a less effective conjugation between the various building blocks. In this regard, the C≡N stretching vibrations are measured as sharp peaks at 2220 cm^{-1} in both the IR and Raman spectra, indicating a more pronounced triple bond character than in **1b**, and consequently a lower involvement of the CN groups in the overall π-conjugation of the target **1a** chromophore.

We also analyzed the thermal evolution of the FT-IR spectrum of **1b** from 25 to 170 °C (see Figure 13). No drastic spectral changes were evidenced upon heating the KBr pellet until the highest temperature was reached, but merely an overall and continuous downshift of the IR absorptions (namely, in any case by less than 2−3 cm^{-1}), which could be likely attributed to the thermal expansion of the solid and that may be thereby reflecting the little or negligible effect of the intermolecular interactions on the vibrational potential of this **1b** cross-conjugated system.

On the other hand, solid-state Raman scatterings at 2209, 1500, 1451, and 1394 cm^{-1} (i.e., all of them being associated to skeletal stretching vibrations of C≡N and C═C bonds) upshift to 2218, 1508, 1460, and 1397 cm^{-1}, respectively, upon solution of the **1b** compound in CH_2Cl_2, CH_3CN, or DMSO (see Figure 14). Since the Raman profiles collected for the various dilute solutes are quite similar to each other, it may be concluded that (i) the average conformational distortion of **1b** in solution must be nearly the same in any solvent, and thus the increasing polarity of the surrounding medium does not seemingly enhance the degree of ICT (i.e., which in its turn could be a direct consequence of the undulated and strained structure of the compound subject of study) and (ii) the observation that the ν(CN) Raman scatterings in solution are no longer recorded as a very strong and sharp peak as for the pure solid but as a medium-weak and broad feature with various components suggests that the rotation of the $C{=}C(CN)_2$ acceptor moiety about the $C_\alpha-C_{sp^2}$ bonds with respect to the thienyl−S−CH_2−S−thienyl core could give rise to a statistical equilibrium between different conformers. This hypothesis also meets support in the 8 cm^{-1} upshift underwent by the stretching vibration of the olefinic bond near 1500 cm^{-1} upon the removal of the crystal packing forces. Finally, from the comparison between the solid state and solution Raman spectroscopic data it becomes apparent that the prevailing molecular structure for **1b** should be more flat and conjugated as a pure solid, even at high temperatures, than in any polar or nonpolar solvent. One point that gives support to this conclusion is the fact that the electron density transferred from the electron-rich thienyl−S−CH_2−S−thienyl core to the electron-withdrawing dicyanoethylene group is estimated to lower upon solution to around 0.25 *e* (namely, assuming again the applicability of the data summarized in Figure 1 of ref 57a to the bisthienodithiocins subject of study), a value even smaller than the B3LYP/6-31G** net NPA charge computed for the gas-phase **1b** minimum-energy molecular structure.

IV. Conclusions

The synthesis of a novel cross-conjugated bithienyl chromophore with amphoteric redox behavior is reported. The analysis at the molecular scale of its structure/property relationships has been performed by means of selected spectroscopic techniques (electron absorption and IR and Raman spectroscopies) whose data are compared and combined with electrochemistry and supported by DFT quantum chemical calculations. The whole set of data has been compared with those obtained for another isomeric push−pull chromophore which however is not longer cross-conjugated.

The main aim of this research was to design novel π-conjugated chromophores suited for electropolymerization in order to afford new polymeric structures with multifunctional properties. However, the target **1b** cross-conjugated compound did not lead to good polymers due to overoxidation. The next step to avoid degradation of the monomer should be that of trying to reduce its first oxidation potential. A feasible strategy to this end should be the substitution of the free β-positions of the thienyl rings by donor groups (such as MeO or others) or by solubilizing long alkyl side chains. An alternative synthetic route could be the replacement of the single thienyl rings at either side of the push−pull chromophore by longer α-linked oligothienyl chains. The copolymerization of this type of cross-conjugated structures with other usual α-oligoheteroaromatics should also deserve attention, in order to develop new π-conjugated polymers with a likely multifunctionality.

This manuscript illustrates the importance of developing novel types of π-conjugated organic structures. Physicochemical investigations of these materials at the molecular scale can provide fundamental new insight into mechanisms of π-conjugation and the interplay between the push−pull character and cross-conjugation observed for the **1b** bisthienodithiocin subject of study. On the basis of the results reported here, it is suggested that the design of the chemical structures of these compounds

may be further improved as to provide promising advanced molecular materials with high-performance electronic and optical properties.

Acknowledgment. Research at the University of Málaga was supported by the Ministerio de Educación y Ciencia (MEC) of Spain through Project CTQ2006-14987-C02-01 and by the Junta de Andalucía for funding our FQM-0159 scientific group and for the Project P06-FQM-01678. R.P.O. and R.M.O. are also grateful to MEC and Junta de Andalucía for their personal doctoral grants. V.G.N., V.V.S., and E.S.B. are grateful for financial support from the Russian Foundation for Basic Research (Grant N 03-03-32024-a) and Russian Science Support Foundation.

Supporting Information Available: Synthetic details for compounds **1**, **2**, **3**, and **4**; ^{1}H NMR and ^{13}C spectra for compounds **1**, **2**, **3**, and **4**; X-ray crystallographic data for compounds **1a** and **1b**; full author list for ref 25. This material is available free of charge via the Internet at http://pubs.acs.org.

References and Notes

(1) (a) *Handbook of Conducting Polymers*, 2nd ed.; Skotheim, T. A., Elsenbaumer, R. L., Reynolds, J. R., Eds.; Marcel Dekker: New York, 1998. (b) *Handbook of Organic Conductive Molecules and Polymers*; Nalwa, H. S., Ed.; Wiley: Chichester, U.K., 1997; Vols. 1−4.

(2) Shirakawa, H. In ref 1a; pp 197−208.

(3) (a) Burroughes, J. H.; Bradley, D. C.; Brown, A. R.; Marks, R. N.; McKay, K.; Friend, R. H.; Burn, P. L.; Holmes, A. B. *Nature* **1990**, *347*, 539. (b) Sheats, J. R.; Antoniadis, H.; Hueschen, M.; Leonard, W.; Miller, J.; Moon, R.; Roitman, D.; Stocking, A. *Science* **1996**, *273*, 884. (c) Friend, R. H.; Gymer, A. B.; Holmes, A. B.; Burroughes, J. H.; Marks, R. N.; Taliani, C.; Bradley, D. C.; Santos, D. A. D.; Bredas, J. L.; Logdlund, M.; Salanek, W. R. *Nature* **1999**, *397*, 121. (d) *Photonic Polymer Systems: Fundamentals, Methods and Applications*; Wise, D. L., Wnek, G. E., Trantolo, D. J., Cooper, T. M., Gresser, J. D., Eds.; Marcel Dekker: New York, 1998.

(4) (a) McCullough, R. D. *Adv. Mater*. **1998**, *10*, 93. (b) *Handbook of Oligo and Polythiophenes*; Fichou, D., Ed.; Wiley-VCH: Weinheim, Germany, 1998. (c) Andersson, M. R.; Thomas, O.; Mammo, W.; Svenson, M.; Theander, M.; Inganäs, O. *J. Mater. Chem*. **1999**, *9*, 1933.

(5) (a) *Electronic Materials: The Oligomeric Approach*; Müllen, K., Wegner, G., Eds.; Wiley-VCH: Weinheim, Germany, 1998. (b) Roncali, J. *J. Mater. Chem*. **1997**, *7*, 2307. (c) Horowitz, G. *J. Mater. Chem*. **1999**, *9*, 2021.

(6) Dewar, M. J. S. In *Modern Models of Bonding and Delocalization*; Liebman, J. F., Greenberg, A., Eds.; VCH: Weinheim, Germany, 1988; pp 2−61.

(7) Winstein, S. *Spec. Publ.—R. Chem. Soc*. **1967**, *21*, 5.

(8) Miller, R. D.; Michl, J. *Chem. Rev*. **1989**, *89*, 1359.

(9) Hoogesteger, F. J.; van Walree, C. A.; Jenneskens, L. W.; Roest, M. R.; Verhoeven, J. W.; Schuddeboom, W.; Piet, J. J.; Warman, J. M. *Chem. Eur. J*. **2000**, *6*, 2948.

(10) Bakkers, E. P. A. M.; Marsman, A. W.; Jenneskens, L. W.; Vanmaekelbergh, D. *Angew. Chem.* **2000**, *112*, 2385.; *Angew. Chem., Int. Ed.* **2000**, *39*, 2297.

(11) Fang, M. C.; Watanabe, A.; Matsuda, M. *Macromolecules* **1996**, *29*, 6807.

(12) Kwak, G.; Matsuda, M. *Macromolecules* **2002**, *35*, 4138.

(13) van Walree, C. A.; Kooijman, H.; Spek, A. L.; Zwikker, J. W.; Jenneskens, L. W. *J. Chem. Soc., Chem. Commun*. **1995**, 35.

(14) van Walree, C. A.; Roest, M. R.; Schuddeboom, W.; Jenneskens, L. W.; Verhoeven, J. W.; Warman, J. M.; Kooijman, H.; Spek, A. L. *J. Am. Chem. Soc*. **1996**, *118*, 8395.

(15) García Martínez, A.; Osío Barcina, J.; de Fresno Cerezo, A.; Rojo, G.; Agulló-López, F. *J. Phys. Chem. B* **2000**, *104*, 43.

(16) Phelan, N. F.; Orchin, M. *J. Chem. Educ.* **1968**, *45*, 633.

(17) (a) Fiedler, S.; Rowan, D. D.; Sherburn, M. S. *Angew. Chem.* **2000**, *112*, 4501. (b) Fiedler, S.; Rowan, D. D.; Sherburn, M. S. *Angew. Chem., Int. Ed. Engl.* **2000**, *39*, 4331.

(18) Bryce, M. R.; Coffin, M. A.; Skabara, P. J.; Moore, A. J.; Batsanov, A. S.; Howard, J. A. K. *Chem. Eur. J*. **2000**, *6*, 1955.

(19) Tykwinski, R. R. *Chem. Commun.* **1999**, 905.

(20) Zhao, Y.; McDonald, R.; Tykwinski, R. R. *Chem. Commun.* **2000**, 77.

(21) Bronsted Nielsen, M.; Schreiber, M.; Baek, Y. G.; Seisler, P.; Lecomte, S.; Boudon, C.; Tykwinski, R. R.; Gisselbrecht, J. P.; Gramlich, V.; Skinner, P. J.; Bosshard, C.; Günter, P.; Gross, M.; Diederich, F. *Chem. Eur. J*. **2001**, *7*, 3263.

(22) Boldi, A. M.; Anthony, J.; Gramlich, V.; Knobler, C. B.; Boudon, C.; Gisselbrecht, J. P.; Gross, M.; Diederich, F. *Helv. Chim. Acta* **1995**, *78*, 779.

(23) Nenajdenko, V. G.; Sumerin, V. V.; Chernichenko, K. Y.; Balenkova, E. S. *Org. Lett*. **2004**, *6*, 3437.

(24) Sheldrich, G. M. *SHELXL-97 Program Package*; University of Göttingen: Göttingen, Germany, 1997.

(25) Frisch, M. J.; et al. *Gaussian 03*, revision B.04; Gaussian Inc.: Pittsburgh, PA, 2003.

(26) Becke, A. D. J. *Chem. Phys.* **1993**, *98*, 1372.

(27) Francl, M. M.; Pietro, W. J.; Hehre, W. J.; Binkley, J. S.; Gordon, M. S.; Defrees, D. J.; Pople, J. A. *J. Chem. Phys.* **1982**, *77*, 3654.

(28) (a) Runge, E.; Gross, E. K. U. *Phys. Rev. Lett.* **1984**, *52*, 997. (b) Gross, E. K. U.; Kohn, W. *Adv. Quantum Chem.* **1990**, *21*, 255. (c) Gross, E. K. U.; Ullrich, C. A.; Gossman, U. J. In *Density Functional Theory*; Gross, E. K. U., Driezler, R. M., Eds.; Plenum Press: New York, 1995; p149.

(29) Casida, M. E. In *Recent Advances in Density Functional Methods, Part I*; Chong, D. P., Ed.; World Scientific: Singapore, 1995; p 155.

(30) Koch, W.; Holthausen, M. C. *A Chemist's Guide to Density Functional Theory*; Wiley-VCH: Weinheim, Germany, 2000.

(31) Hsu, C.-P.; Hirata, S.; Head-Gordon, M. *J. Phys. Chem. A* **2001**, *105*, 451.

(32) (a) Hirata, S.; Lee, T. J.; Head-Gordon, M. *J. Chem. Phys*. **1999**, *111*, 8904. (b) Heinze, H. H.; Görling, A.; Rösch, N. *J. Chem. Phys*. **2000**, *113*, 2088. (c) Weisman, J. L.; Lee, T. J.; Head-Gordon, M. *Spectrochim. Acta A* **2001**, *57*, 931. (d) Hirata, S.; Head-Gordon, M.; Szcsepanski, J.; Vala, M. *J. Phys. Chem. A* **2003**, *107*, 4940. (e) Grimme, S.; Parac, M. *ChemPhysChem* **2003**, *3*, 292. (f) Parac, M.; Grimme, S. *Chem. Phys*. **2003**, *292*, 11.

(33) Halasinski, T. M.; Weisman, J. L.; Ruiterkamp, R.; Lee, T. J.; Salama, F.; Head-Gordon, M. *J. Phys. Chem. A* **2003**, *107*, 3660.

(34) Bauernschmitt, R.; Ahlrichs, R.; Heinrich, F. H.; Kappes, M. M. *J. Am. Chem. Soc*. **1998**, *120*, 5052.

(35) (a) Pogantsch, A.; Heimel, G.; Zojer, E. *J. Chem. Phys*. **2002**, *117*, 5921. (b) Hutchison, G. R.; Ratner, M. A.; Marks, T. J. *J. Chem. Phys. A* **2002**, *106*, 10596. (c) Casado, J.; Pappenfus, T. M.; Miller, L. L.; Mann, K. R.; Ortí, E.; Viruela, P. M.; Pou-Amérigo, R.; Hernández, V.; López Navarrete, J. T. *J. Am. Chem. Soc*. **2003**, *125*, 2524.

(36) (a) van Gisbergen, S. J. A.; Rosa, A.; Ricciardi, G.; Baerends, E. J. *J. Chem. Phys*. **1999**, *111*, 2499. (b) Nguyen, K. A.; Pachter, R. *J. Chem. Phys*. **2001**, *114*, 10757. (c) Jaworska, M.; Kazibut, G.; Lodowski, P. *J. Phys. Chem. A* **2003**, *107*, 1339.

(37) Yamaguchi, Y. *J. Chem. Phys*. **2002**, *117*, 9668.

(38) Pou-Amérigo, R.; Viruela, P. M.; Viruela, R.; Rubio, M.; Ortí, E. *Chem. Phys. Lett*. **2002**, *352*, 491.

(39) Portmann, S.; Lüthi, H. P. *Chimia* **2000**, *54*, 766−770.

(40) Scott, A. P.; Radom, L. *J. Phys. Chem*. **1996**, *100*, 16502.

(41) Ham, J.; Yang, I.; Kang, K. *J. Org. Chem*. **2004**, *69*, 3236.

(42) Uri, M.; Hörnfeldt, A.-B. *Tetrahedron Lett*. **1970**, *11*, 5219.

(43) Lucas, P.; Mehdi, N. E.; Ho, H. A.; Bélanger, D.; Breau, L. *Synthesis* **2000**, 1253.

(44) Takahashi, K.; Kobayashi, K. *J. Org. Chem*. **2000**, *65*, 2577.

(45) *Handbook of Chemistry and Physics*, 82nd ed.; Lide, D. R., Ed.; CRC: Boca Raton, FL, 2001.

(46) (a) Alemán, C.; Juliá, L. *J. Phys. Chem*. **1996**, *100*, 14661. (b) Irle, S.; Lischka, H. *J. Chem. Phys*. **1997**, *107*, 3021. (c) Moro, G.; Scalmani, G.; Cossentino, U.; Pitea, D. *Synth. Met*. **1998**, *92*, 69.

(47) Casado, J.; Ponce Ortiz, R.; Ruiz Delgado, M. C.; Azumi, R.; Oakley, R. T.; Hernandez, V.; Lopez Navarrete, J. T.; Tanaka, S.; Yamashita, Y. *J. Phys. Chem. B* **2005**, *109*, 10115.

(48) Ruiz Delgado, M. C.; Hernandez, V.; Lopez Navarrete, J. T.; Tanaka, S.; Yamashita, Y. *J. Phys. Chem. B* **2004**, *108*, 2516.

(49) (a) Sakamoto, Y.; Komatsu, S.; Suzuki, T. *J. Am. Chem. Soc*. **2001**, *123*, 4643. (b) Sakamoto, Y.; Komatsu, S.; Suzuki, T. *Synth. Met*. **2003**, *133*, 361.

(50) Klokkenburg, M.; Lutz, M.; Spek, A. L.; van der Maas, J. H.; van Walree, C. A. *Chem. Eur. J*. **2003**, *9*, 3544.

(51) Pysh, E. S.; Yang, N. C. *J. Am. Chem. Soc*. **1963**, *85*, 2124.

(52) (a) Del Zoppo, M.; Tommasini, M.; Castiglioni, C.; Zerbi, G. *Chem. Phys. Lett*. **1998**, *287*, 100. (b) Hernandez, V.; Casado, J.; Effenberger, F.; Lopez Navarrete, J. T. *J. Chem. Phys*. **2000**, *112*, 5105. (c) Gonzalez, M.; Segura, J. L.; Seoane, C.; Martin, N.; Garin, J.; Orduna, J.; Alcala, R.; Villacampa, B.; Hernandez, V.; Lopez Navarrete, J. T. *J. Org. Chem*. **2001**, *66*, 8872. (d) Ruiz Delgado, M. C.; Hernandez, V.; Casado, J.; Lopez Navarrete, J. T.; Raimundo, J. M.; Blanchard, P.; Roncali, J. *Chem. Eur. J*. **2003**, *9*, 3670. (e) Casado, J.; Hernandez, V.; Kim, O. K.; Lehn, J. M.; Lopez Navarrete, J. T.; Delgado Ledesma, S.; Ponce Ortiz, R.; Ruiz Delgado, M. C.; Vida, Y.; Perez-Inestrosa, E. *Chem. Eur. J*. **2004**, *10*, 3805.

(53) (a) Ponce Ortiz, R.; Ruiz Delgado, M. C.; Casado, J.; Hernandez, V.; Kim, O. K.; Woo, H. Y.; Lopez Navarrete, J. T. *J. Am. Chem. Soc.*

2004, *126*, 13363. (b) Moreno Castro, C.; Ruiz Delgado, M. C.; Hernandez, V.; Shirota, Y.; Casado, J.; Lopez Navarrete, J. T. *J. Phys. Chem. B* **2002**, *106*, 7163. (c) Moreno Castro, C.; Ruiz Delgado, M. C.; Hernandez, V.; Hotta, S.; Casado, J.; Lopez Navarrete, J. T. *J. Chem. Phys.* **2002**, *116*, 10419.

(54) (a) Hernández, V.; Casado, J.; Ramírez, F. J.; Zotti, G.; Hotta, S.; López Navarrete, J. T. *J. Chem. Phys.* **1996**, *104*, 9271. (b) Hernández, V.; Hotta, S.; López Navarrete, J. T. *J. Chem. Phys.* **1998**, *109*, 2543. (c) Hernández, V.; Calvo Losada, S.; Casado, J.; Higuchi, H.; López Navarrete, J. T. *J. Phys. Chem. A* **2000**, *104*, 661.

(55) (a) Casado, J.; Hotta, S.; Hernández, V.; López Navarrete, J. T. *J. Phys. Chem. A* **1999**, *103*, 816. (b) Hernández, V.; Casado, J.; Ramírez, F. J.; Alemany, L. J.; Hotta, S.; López Navarrete, J. T. *J. Phys. Chem.* **1996**, *100*, 289. (c) Hernández, V.; Muguruma, H.; Hotta, S.; López Navarrete, J. T. *J. Phys. Chem. A* **2000**, *104*, 735. (d) Casado, J.; Hernández, V.; Hotta, S.; López Navarrete, J. T. *J. Chem. Phys.* **1998**, *109*, 10419.

(56) (a) Casado, J.; Hernández, V.; Hotta, S.; López Navarrete, J. T. *Adv. Mater*. **1998**, *10*, 1458. (b) Casado, J.; Katz, H. E.; Hernández, V.; López Navarrete, J. T. *J. Phys. Chem. B* **2002**, *106*, 2488. (c) Casado, J.; Miller, L. L.; Mann, K. R.; Pappenfus, T. M.; Hernández, V.; López Navarrete, J. T. *J. Phys. Chem. B* **2002**, *106*, 3597.

(57) (a) Chappell, J. S.; Bloch, A. N.; Bryden, W. A.; Maxfield, M.; Poehler, T. O.; Cowan, D. O. *J. Am. Chem. Soc*. **1981**, *103*, 2442. (b) Diaz, A. F.; Crowley, J.; Bargon, J.; Gardini, G. P.; Torrance, J. B. *J. Electroanal. Chem*. **1981**, *121*, 355.

(58) (a) Yui, K.; Aso, Y.; Otsubo, T.; Ogura, F. *J. Chem. Soc., Chem. Commun*. **1987**, 1816. (b) Yui, K.; Aso, Y.; Otsubo, T.; Ogura, F. *Bull. Chem. Soc. Jpn*. **1989**, *62*, 1539. (c) Yui, K.; Ishida, H.; Aso, Y.; Otsubo, T.; Ogura, F.; Kawamoto, A.; Tanaka, J. *Bull. Chem. Soc. Jpn*. **1989**, *62*, 1547. (d) Ishida, H.; Yui, K.; Aso, Y.; Otsubo, T.; Ogura, F. *Bull. Chem. Soc. Jpn*. **1990**, *63*, 2828. (e) Ogura, F.; Otsubo, T.; Aso, Y. *Sulfur Rep.* **1992**, *11*, 439. (f) Yoshida, S.; Fujii, M.; Aso, Y.; Otsubo, T.; Ogura, F. *J. Org. Chem*. **1994**, *59*, 3077. (g) Higuchi, H.; Nakayama, T.; Koyama, H.; Ojima, J.; Wada, T.; Sasabe, H. *Bull. Chem. Soc. Jpn*. **1995**, *68*, 2363. (h) Higuchi, H.; Yoshida, S.; Uraki, Y.; Ojima, J. *Bull. Chem. Soc. Jpn*. **1998**, *71*, 2229. (i) Casado, J.; Miller, L. L.; Mann, K. R.; Pappenfus, T. M.; Higuchi, H.; Orti, E.; Milian, B.; Pou-Amerigo, R.; Hernandez, V.; Lopez Navarrete, J. T. *J. Am. Chem. Soc.* **2002**, *124*, 12380. (j) Casado, J.; Pappenfus, T. M.; Mann, K. R.; Ortí, E.; Viruela, P. M.; Millián, B.; Hernández, V.; López Navarrete, J. T. *ChemPhysChem* **2004**, *5*, 529.

(59) Chapell, J. S.; Bloch, A. N.; Bryden, W. A.; Maxfield, M.; Poehler, T. O.; Cowan, D. O. *J. Am. Chem. Soc.* **1981**, *103*, 2442.

(60) (a) Takenaka, T. *Spectrochim. Acta A* **1971**, *27*, 1735. (b) Girlando, A.; Pecile, C. *Spectrochim. Acta A* **1973**, *29*, 1859. (c) Faulques, E.; Leblanc, A.; Molini, P.; Decoster, M.; Conan, F.; Guerchais, J. E.; Sala-Sala, J. *Spectrochim. Acta A* **1995**, *51*, 805.